

3DMR osseous reconstructions of the shoulder using a gradient-echo based two-point Dixon reconstruction: a feasibility study

Soterios Gyftopoulos · Avner Yemin · Thomas Mulholland · Michael Bloom · Pippa Storey · Christian Geppert · Michael P. Recht

Received: 6 June 2012 / Revised: 29 June 2012 / Accepted: 2 July 2012 / Published online: 25 July 2012
© ISS 2012

Abstract

Objective To create 3DMR osseous models of the shoulder similar to 3DCT models using a gradient-echo-based two-point/Dixon sequence.

Materials and methods CT and 3TMR examinations of 7 cadaveric shoulders were obtained. Glenoid defects were created in 4 of the cadaveric shoulders. Each MR study included an axial Dixon 3D-dual-echo-time T1W-FLASH (acquisition time of 3 min/30 s). The water-only image data from the Dixon sequence and CT data were post-processed using 3D software. The following measurements were obtained on the shoulders: surface area (SA), height/width of the glenoid and humeral head, and width of the biceps groove. The glenoid defects were measured on imaging and compared with measurements made on *en face* digital photographs of the glenoid fossae (reference standard). Paired *t* tests/ANOVA were used to assess the differences between the imaging modalities.

Results The differences between the glenoid and humeral measurements were not statistically significant (cm): glenoid SA 0.12 ± 0.04 ($p=0.45$) and glenoid width 0.13 ± 0.06 ($p=0.06$) with no difference in glenoid height measurement; humeral head SA 0.07 ± 0.12 ($p=0.42$), humeral head height 0.03 ± 0.06 ($p=0.42$), humeral head width 0.07 ± 0.06 ($p=0.18$), and biceps groove width 0.02 ± 0.01 ($p=0.07$). The mean/standard deviation difference between the reference standard and 3DMR measurements was 0.25 ± 0.96 %/ 0.30 ± 0.14 mm; 3DCT 0.25 ± 0.96 / 0.75 ± 0.39 mm. There was no

statistical difference between the measurements obtained on 3DMR and 3DCT (percentage, $p=0.45$; mm, $p=0.20$).

Conclusion Accurate 3D osseous models of the shoulder can be produced using a 3D two-point/Dixon sequence and can be added to MR examinations with a minor increase in imaging time, used to quantify glenoid loss, and may eliminate the need for pre-surgical CT examinations.

Keywords Shoulder dislocation · 3DMR · Glenoid bone loss

Introduction

High-resolution CT imaging with 3D reconstructions is a helpful tool in the evaluation of multiple musculoskeletal conditions including recurrent shoulder dislocation and femoroacetabular impingement [1–7]. The 3D reconstructions are favored by some surgeons because they allow for improved conceptualization of the osseous anatomy in these conditions compared with 2D imaging modalities. In patients with a history of recurrent shoulder dislocation and/or evidence of bone loss on radiographs in the setting of shoulder dislocation, 3DCT images are obtained to evaluate and quantify the amount of bone loss along the glenoid or humeral head to guide treatment selection [8–10]. MRI is usually also ordered in the setting of recurrent dislocation as it remains the imaging gold standard for the evaluation of the soft tissue injuries found in this condition.

The ability to create accurate 3D osseous reconstructions from MR data would be advantageous for the surgeon and patient as well as help to limit costs. There would be one less study to order by the physician, one less study to undergo by the patient, and the patient would be spared the radiation dose that comes with undergoing a CT examination. The purpose of

S. Gyftopoulos (✉) · A. Yemin · T. Mulholland · M. Bloom · P. Storey · C. Geppert · M. P. Recht
Department of Radiology, NYU Langone Medical Center,
560 First Avenue,
New York, NY 10016, USA
e-mail: Soterios20@gmail.com

this study is to see if it is possible to create 3D MR osseous models of the shoulder that are similar in shape and accuracy to 3D CT models using a unique MR method, and to see if these models can be used to accurately quantify glenoid bone loss.

Materials and methods

3DMR/3DCT comparison

Three shoulders from fresh-frozen cadavers (3 females; mean age=52 years) were used for the study, and labeled #1–3. Cadaver #3 had a prior anterior labral repair. Each specimen underwent CT (SOMATOM Sensation 40; Siemens, Munich, Germany) and MRI (MAGNETOM SKYRA 3T; Siemens, Munich, Germany) examinations. The CT protocol consisted of volumetric 3-mm acquisitions through the shoulder using the following parameters: 120 kV, 280 mAs, pitch 0.9, 0.6-mm collimation, and a smooth algorithm. The MR protocol consisted of an axial 3D dual echo-time T1-weighted FLASH acquisition with Dixon-based water–fat separation through the shoulder using a four-channel transmit–receive phased array shoulder coil and the following parameters: TR 10, TE 2.45/3.7, field of view of 200 mm, acquired voxel size 1.0×1.0×1.4 mm, reconstructed voxel size 1.0×1.0×1.0 mm, flip angle 9°, matrix 192×192, bandwidth 400 Hz/pixel, acquisition time of 3 min and 28 s, number of partitions=120 and a slice thickness of 1 mm.

The MR data from each shoulder was then post-processed using standard subtraction software on a *syngo* MMWP workstation (VB 3oE, Siemens). The source images were the water-only images obtained from the Dixon sequence. The lowest mean signal intensity (water_min) from multiple ROI [5–10] of the soft tissues surrounding the osseous structures was used as a constant to calculate a subtraction image where the pixel values are subtracted from this constant (water_min – SI(i), with negative values being set to zero). This resulted in inverted images with signal-void soft tissue structures and signal-avid osseous structures (Fig. 1). One MR technologist with 12 years of experience completed the subtraction portion of the post-processing. The subtracted Dixon images were then manually segmented and 3D models were generated (Tera Recon software [4.4.5.36.2068]). In addition, 3DCT osseous models were also generated using the same manual segmentation and 3D software tools. The 3D post-processing was done by one of two CT technologists (with 10 years and 3 years of 3D post-processing experience respectively).

One board certified musculoskeletal radiologist with 3 years of experience completed all the CT and MR measurements. The following measurements were obtained on each MR and CT 3D shoulder reconstruction and then compared: height, width and surface area of the glenoid and humerus and width of the biceps groove. The glenoid measurements were

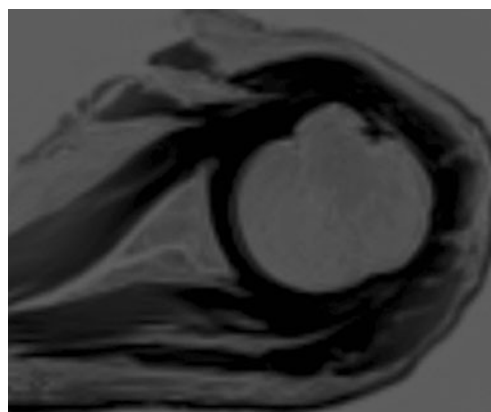


Fig. 1 Subtracted Dixon image of a cadaveric left shoulder. A post-processed, subtracted Dixon image from intact cadaver no. 1 demonstrates the contrast between the signal-avid osseous structures and signal-void surrounding soft tissue structures

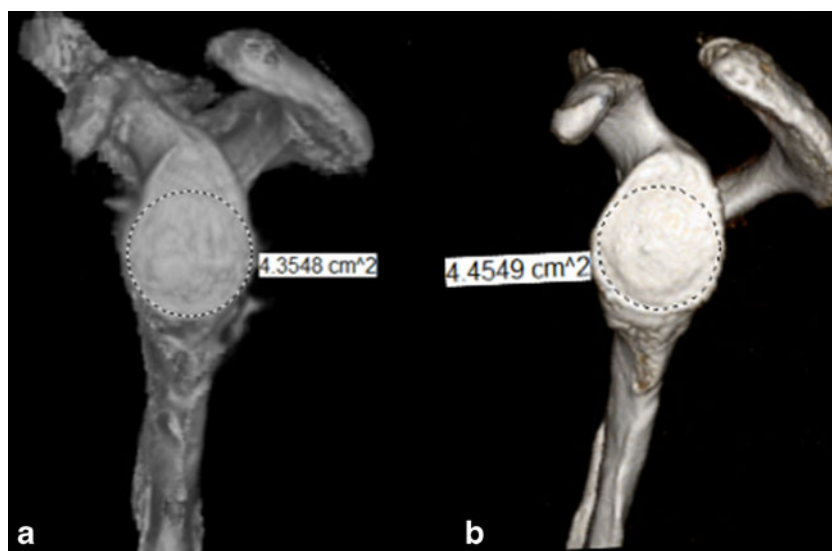
obtained along the articular surface of the glenoid in the lateral view (Fig. 2). The humeral head measurements were obtained along its anterior surface. Using a best-fit circle around the margins of the humeral head, the surface area of that portion of the humeral head was automatically calculated using Philips Isite software (Fig. 3). The biceps groove measurement was obtained at the midpoint of the groove. The CT measurements were done first, in random order. The MR measurements were done 4 weeks after the CT measurements, also in random order. Paired sample *t* tests were used to compare the measurements obtained on the 3DMR models with those obtained on the 3DCT models.

Glenoid bone loss quantification

Four shoulders from fresh-frozen cadavers (1 male and 3 females; mean age=76 years) were used for this portion of the study. The specimens were frozen at –9 °C and thawed overnight at room temperature for the experiment. The surrounding capsuloligamentous structures were maintained while the remainder of the soft tissues and humerus were removed and discarded. Each specimen was prepared in the same manner and numbered 1–4. None of the specimen demonstrated pre-existing anterior bone loss and therefore all the glenoids were included in our study. A custom clamp was assembled to secure each individual scapula. A bone saw was used to create a straight vertical cut along the anterior margin of the glenoid at the 3 o'clock position at a predetermined distance from the glenoid bare spot. Images of the en-face/lateral view of the glenoids were then obtained with an adjacent measuring ruler using a digital camera (Canon rebel XSi; Canon, Japan). The osteotomies were done by one sports medicine orthopedic surgeon with 16 years of experience.

Each specimen underwent CT (SOMATOM Sensation 40; Siemens, Munich, Germany) and MRI (MAGNETOM

Fig. 2 3DMR and 3DCT glenoid reconstructions. Lateral views of **a** 3DMR and **b** 3DCT reconstructions of the scapula of intact cadaver no. 1 demonstrate a 0.1-cm² difference between the glenoid articular surface area measurements. No statistically significant difference was found when comparing the MR and CT glenoid surface area measurements of all three cadavers



SKYRA 3T; Siemens, Munich, Germany) examinations with the same protocols as stated before. 3DMR and 3DCT models were then produced using the same technique as above. Using a revised circle method technique and Philips Isite software, one reader analyzed the data (Fig. 4) [5]. The reader measured the size of the glenoid defect using a lateral view of the glenoid on the 3D reconstructions. A line was drawn along the long axis of the glenoid from the supraglenoid tubercle through the inferior aspect of the inferior glenoid rim perpendicular to the transverse plane of the glenoid, marking the center of the glenoid. A best-fit circle was then placed along the inferior portion of the glenoid using the intact posterior and inferior margins as a guide and making sure that the center of the circle overlay the vertical line. A line was drawn through the center of the circle between the anterior and posterior margins representing an estimate of the intact glenoid's AP diameter. The

glenoid defects were measured in terms of width (mm) and percentage bone loss in the AP dimension ($1 - ((\text{width of glenoid} - \text{width of defect}) / \text{estimated width of glenoid})$). The MR measurements were done first, in random order. The CT measurements were done next, also in random order, 2 weeks after the MR measurements.

Using the en face digital photographs of the glenoid fossae, the glenoid bone loss was measured using a revised glenoid bare spot method by the musculoskeletal radiologist (Fig. 4) [9, 11]. The bare area was identified on the image. The distances from the bare area to the posterior and anterior glenoid margins were measured. The difference between these two measurements constituted the amount of glenoid bone loss in millimeters. The percentage of glenoid bone loss was calculated using the following equation: $[(\text{posterior distance} - \text{anterior distance}) / (2 \times \text{posterior distance})] \times 100\%$. The measurements on the digital photographs were carried out in a



Fig. 3 3DMR and 3DCT humerus reconstructions. Frontal views of **a** 3DMR and **b** 3DCT reconstructions of the proximal humerus of cadaver no. 1 demonstrate a 0.25-cm² difference between the humeral head surface area measurements and a 0.4-mm difference in the

humeral head width measurements. No statistically significant difference was found when comparing the MR and CT humeral head surface area measurements and humeral head width of all three cadavers

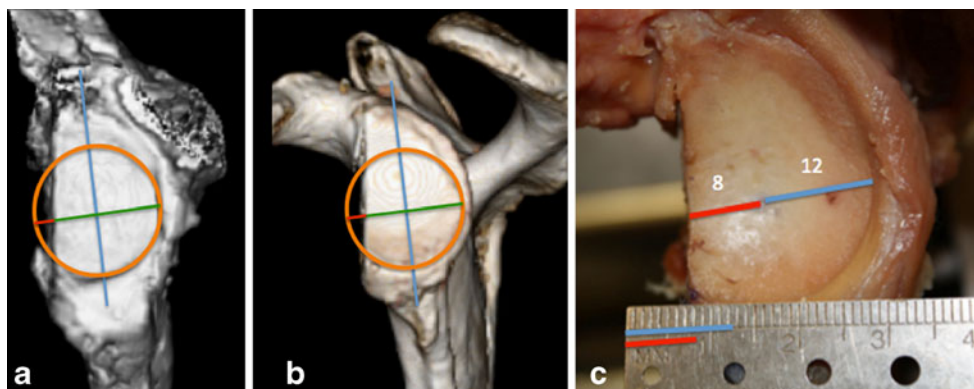


Fig. 4 Glenoid bone quantification. Lateral **a** 3DMR and **b** 3DCT images of the same glenoid demonstrate the steps used to estimate glenoid loss on imaging. A line was drawn (*blue*) along the long axis of the glenoid from the supraglenoid tubercle, marking the center of the glenoid. A best-fit circle (*orange*) was then placed along the inferior portion of the glenoid using the intact posterior and inferior margins as a guide and making sure that the center of the circle overlays the vertical line. A line (*green*) was drawn through the center of the circle between the anterior and posterior margins representing an estimate of the intact glenoid's width. The glenoid defects (*red line*) were measured in terms of width (mm) and percentage bone loss in the AP dimension ($1 - ((\text{width of glenoid} - \text{width of defect}) / \text{estimated width of$

glenoid)). The defect measured 4.4 mm on 3DMR, which equaled 18 % loss of the glenoid width, while measuring 5.3 mm and equaling 18 % loss of width as well on 3DCT. **c** Digital image of the same glenoid from Fig. 3 demonstrates the steps used for the revised bare spot method. The distances from the bare area to the posterior (*blue line*) and anterior glenoid (*red line*) margins were measured. The difference between these two measurements constituted the amount of glenoid bone loss in millimeters. The percentage glenoid bone loss was calculated using the following equation: $[(\text{posterior distance} - \text{anterior distance}) / (2 \times \text{posterior distance})] \times 100 \%$. The defect measured 4 mm, resulting in a 17 % loss of the glenoid width

random order, 2 weeks after the CT measurements were completed. These measurements were used as the reference standard. Two-way analysis of variance (ANOVA) was used to assess the differences among modalities.

Results

3DMR/3DCT comparison

The average surface area (SA) of the glenoid on the 3DMR model was $4.65 \pm 0.35 \text{ cm}^2$, average height $3.47 \pm 0.15 \text{ cm}$, and average width $2.37 \pm 0.06 \text{ cm}$. The surface area on the 3DCT model was $4.72 \pm 0.32 \text{ cm}^2$, the average height $3.47 \pm 0.15 \text{ cm}$, and average width $2.5 \pm 0.1 \text{ cm}$. The differences between these two groups of measurements were not statistically significant: glenoid SA $0.12 \pm 0.04 \text{ cm}^2$ ($P=0.45$) and glenoid width $0.13 \pm 0.06 \text{ cm}$ ($P=0.06$). There was no difference between the measurements of the glenoid height ($P=1$; Table 1).

The average surface area (SA) of the humeral head on the 3DMR model was $15.33 \pm 1.57 \text{ cm}^2$, humeral height $4.17 \pm 0.21 \text{ cm}$, humeral width $4.40 \pm 0.17 \text{ cm}$, and biceps groove width $0.49 \pm 0.09 \text{ cm}$. The average surface area (SA) of the humeral head on the 3DCT model was $15.27 \pm 1.61 \text{ cm}^2$, humeral height $4.13 \pm 0.25 \text{ cm}$, humeral width $4.47 \pm 0.21 \text{ cm}$, and biceps groove width $0.50 \pm 0.08 \text{ cm}$. The differences between these two groups of measurements were not statistically significant: humeral head SA $0.07 \pm 0.12 \text{ cm}^2$ ($p=0.42$), humeral head height $0.03 \pm 0.06 \text{ cm}$ ($p=0.42$), humeral head width $0.07 \pm 0.06 \text{ cm}$ ($p=0.18$), and biceps groove width $0.02 \pm 0.01 \text{ cm}$ ($p=0.07$; Table 1).

Glenoid bone loss quantification

The percentages and widths of glenoid defects measured on the digital images of the glenoids ranged between 9 and 23 % and between 2 and 5 mm with an average of 16 % and

Table 1 Paired sample *t* tests were used to compare the average measurements (cm) obtained on the 3DMR models with those obtained on the 3DCT models

Measurement	3DMRI	3DCT	Difference	<i>p</i> value
Glenoid surface area	4.65 ± 0.35	4.72 ± 0.32	0.12 ± 0.04	0.45
Glenoid height	3.47 ± 0.15	3.47 ± 0.15	0	1
Glenoid width	2.37 ± 0.06	2.5 ± 0.1	0.13 ± 0.06	0.06
Humeral surface area	15.33 ± 1.57	15.27 ± 1.61	0.07 ± 0.12	0.42
Humeral height	4.17 ± 0.21	4.13 ± 0.25	0.03 ± 0.06	0.42
Humeral width	4.40 ± 0.17	4.47 ± 0.21	0.07 ± 0.06	0.18
Biceps width	0.49 ± 0.09	0.50 ± 0.08	0.02 ± 0.01	0.07

3.5 mm. The error/observed differences for the 3DMR measurements compared with the reference standard measurements were 0.25 ± 0.96 % and 0.30 ± 0.14 mm, while for the 3DCT measurements they were 0.25 ± 0.96 % and 0.75 ± 0.39 mm. There was no significant difference between the 3DMR and 3DCT measurements (percentage, $p=0.45$; mm, $p=0.20$).

Discussion

3DCT reconstructions play an important role in the evaluation of multiple musculoskeletal abnormalities, including patients with recurrent shoulder dislocation and femoroacetabular impingement. They have been found to be useful in pre-surgical planning, providing an accurate representation of the location and morphology of the osseous anatomy, as well as the opportunity to quantify the pathology in these clinical scenarios [2, 4–6].

The applied Dixon variant is based on a dual-echo 3D-FLASH technique that exploits the chemical shift difference between water and fat. In-phase and opposed-phase images are acquired and then combined in post-processing to produce water-only and fat-only images. In musculoskeletal imaging, the Dixon-based imaging has primarily functioned as a tool for fat suppression and to evaluate bone marrow [12–17]. Its use in the production of 3D reconstructions of joints is novel, to the best of the authors' knowledge.

There are several advantages to using the 3D FLASH-based Dixon technique as the source images for constructing 3D osseous models. First, the 3D data acquisition allows for isotropic or near-isotropic resolution, which allows rotation of the 3D models. Second, the sequence allows for improved segmentation of the osseous structures from the surrounding soft tissues compared with conventional MR sequences. Subtracting the signal of every pixel in the images from the lowest mean signal intensity of the surrounding non-fat soft tissue, i.e., the constant, results in intensity values that are equal to zero or below in the soft tissues (capsule and musculature) surrounding the bones of interest. Negative intensity values cannot be displayed; thus, they are set to zero. On the other hand, the signal in the osseous structures is on average lower than the lowest mean signal intensity (water_min) of the soft tissues. This leads to persistent signal in the bones, highest and most uniformly present in the cortices, on the subtracted images and, overall, increased contrast between osseous structures and surrounding soft tissue (Fig. 1). This results in improved segmentation of the images.

The duration of acquisition for the Dixon sequence is approximately 3 min and 30 s, resulting in a minor increase in imaging time. The length of post-processing time averaged approximately 25 min. The subtraction component is

carried out by one of the MR technologists shortly after the study is completed at the MR scanner and typically takes around 1–3 min, based on the technologist's experience. These images then undergo manual segmentation using our 3D software by one of our 3D lab technologists. The post-processing time is greater than the time for 3DCT (which takes 10 min on average). We foresee the difference between these two techniques decreasing over time as the technologists become more familiar with the Dixon sequence and segmentation of the MR data. We are currently working towards a method that will allow for more automated segmentation of the bones, and thus, decreased post-processing time with the goal of equaling or improving on the 3DCT time.

When comparing the 3DCT models with the 3DMR models, there was no statistical difference between the measurements of the intact glenoid with 0.12 cm² difference in glenoid surface area, 0.13 cm difference in glenoid width, and no difference in measurements of the glenoid height. The differences between the 3DCT and 3DMR humeral measurements were not statistically significant either, with a difference of 0.07 cm² in surface area and 0.03 cm difference in height, 0.07 cm in width, and 0.02 cm in the width of the biceps groove. The glenoid bone loss estimates on the 3DMR models were nearly identical to those obtained on the 3DCT, the imaging gold standard. There were minimal differences compared with the measurements obtained on the reference standard digital images using the bare area method, the clinical gold standard: 0.25 %/ 0.30 -mm average difference for 3DMR and 0.25 %/ 0.75 mm average difference for 3DCT. If larger studies confirm the accuracy of 3DMR osseous models, there will no longer be a need for most if not all CTs obtained to evaluate bony morphology for pre-surgical planning. This would result in one less study to undergo by the patient, as well as eliminating the associated CT radiation dose. In addition, the elimination of CT would lead to decreased cost, an important outcome in today's environment.

The accuracy of 3DMR models was also shown by Rathnayaka et al. [18]. Using a multi-threshold segmentation technique, CT and MRI data were converted into 3D models and then validated against reference models of bones digitized using a mechanical contact scanner. The authors found comparable geometric accuracy between 3DMR and 3DCT models. Abebe et al. used 3DMR models to evaluate ACL tunnel placement using different surgical techniques [19]. Other studies have used MR data in combination with CT data to study knee kinematics and models of bone, muscles, ligaments, and cartilage [20, 21].

There are several limitations to this study. First, this was a pilot study with only 7 cadaveric samples. However, we believe that the data demonstrate that the technique is feasible as there were no significant differences in the

measurements between the two modalities. Second, the shoulder data were performed only on cadavers and not live patients. However, cadaveric specimens are routinely utilized as a surrogate for in vivo studies in radiology research. A larger study performed on patients is necessary to confirm and validate our findings and is currently being performed at our institution.

In conclusion, in this pilot study we have shown that accurate 3D osseous models of the shoulder can be produced using a 3D two-point Dixon sequence and may be used to quantify glenoid bone loss. This sequence can be added to conventional MR examinations, with a minor increase in imaging time, and may eventually eliminate the need for pre-surgical CT examinations.

References

1. Abel MF, Sutherland DH, Wenger DR, Mubarak SJ. Evaluation of CT scans and 3-D reformatted images for quantitative assessment of the hip. *J Pediatr Orthop*. 1994;14:48–53.
2. Beaulé PE, Zaragoza E, Motamedi KD, Copelan N, Dorey FJ. Three-dimensional computed tomography of the hip in the assessment of femoroacetabular impingement. *J Orthop Res*. 2005;23:1286–92.
3. Audenaert EA, Baelde N, Huysse W, Vigneron L, Pattyn C. Development of a three-dimensional detection method of cam deformities in femoroacetabular impingement. *Skeletal Radiol*. 2011;40:921–7.
4. Bedi A, Dolan M, Magennis E, Lipman J, Buly R, Kelly BT. Computer-assisted modeling of osseous impingement and resection in femoroacetabular impingement. *Arthroscopy*. 2012;28:204–10.
5. Sugaya H, Moriishi J, Dohi M, Kon Y, Tsuchiya A. Glenoid rim morphology in recurrent anterior glenohumeral instability. *J Bone Joint Surg Am*. 2003;85:878–84.
6. Chuang TY, Adams CR, Burkhardt SS. Use of preoperative three-dimensional computed tomography to quantify glenoid bone loss in shoulder instability. *Arthroscopy*. 2008;24:376–82.
7. Nofsinger C, Browning B, Burkhardt SS, Pedowitz RA. Objective preoperative measurement of anterior glenoid bone loss: a pilot study of a computer-based method using unilateral 3-dimensional computed tomography. *Arthroscopy*. 2011;27:322–9.
8. Itoi E, Lee SB, Berglund LJ, Berge LL, An KN. The effect of a glenoid defect on anteroinferior stability of the shoulder after bankart repair: a cadaveric study. *J Bone Joint Surg Am*. 2000;82:35–46.
9. Lo IK, Perten PM, Burkhart SS. The inverted pear glenoid: an indicator of significant glenoid bone loss. *Arthroscopy*. 2004;20:169–74.
10. Greis PE, Scuderi MG, Mohr A, Bachus KN, Burks RT. Glenohumeral articular contact areas and pressures following labral and osseous injury to the anteroinferior quadrant of the glenoid. *J Shoulder Elbow Surg*. 2002;11:442–51.
11. Burkhart SS, Debeer JF, Tehrany AM, Parten PM. Quantifying glenoid bone loss arthroscopically in shoulder instability. *Arthroscopy*. 2002;18:488–91.
12. Steiner RM, Mitchell DG, Rao VM, Murphy S, Rifkin MD, Burk DL, et al. Magnetic resonance imaging of bone marrow: diagnostic value in diffuse hematologic disorders. *Magn Reson Q*. 1990;6:17–34.
13. Johnson LA, Hoppel BE, Gerard EL, Miller SP, Doppelt SH, Zizow GC, et al. Quantitative chemical shift imaging of vertebral bone marrow in patients with Gaucher disease. *Radiology*. 1992;182:451–2.
14. Gerard EL, Ferry JA, Amrein PC, Harmon DC, McKinstry RC, Hoppel BE, et al. Compositional changes in vertebral bone marrow during treatment for acute leukemia: assessment with quantitative chemical shift imaging. *Radiology*. 1992;183:39–46.
15. Ballon D, Jakubowski AA, Tulipano PK, Graham MC, Schneider E, Aghazadeh B, et al. Quantitative assessment of bone marrow hematopoiesis using parametric magnetic resonance imaging. *Magn Reson Med*. 1998;39:789–800.
16. Maas M, Dijkstra PF, Akkerman EM. Uniform fat suppression in hands and feet through the use of two-point Dixon chemical shift MR imaging. *Radiology*. 1999;210:189–93.
17. Maas M, Hollak CE, Akkerman EM, Aerts JM, Stoker J, Den Heeten GJ. Quantification of skeletal involvement in adults with type I Gaucher's disease: fat fraction measured by Dixon quantitative chemical shift imaging as a valid parameter. *AJR Am J Roentgenol*. 2002;179:961–5.
18. Rathnayaka K, Konstantin IM, Noser H, Volp A, Schuetz MA, Sahama T, et al. Quantification of the accuracy of MRI generated 3D models of long bones compared to CT generated 3D models. *Med Eng Phys*. 2012;34:357–63.
19. Abebe ES, Moorman CT, Dziedzic TS, Spritzer CE, Cothran RL, Taylor DC, et al. Femoral tunnel placement during anterior cruciate ligament reconstruction: an in vivo imaging analysis comparing transtibial and 2-incision tibial tunnel independent techniques. *Am J Sports Med*. 2009;37:1904–11.
20. Moro-oka T-a, Hamai S, Miura H, Shimoto T, Higaki H, Fregly BJ. Can magnetic resonance imaging-derived bone models be used for accurate motion measurement with single-plane three-dimensional shape registration? *J Orthop Res*. 2007;25:867–72.
21. Laura Z, Erik RW, Michael DS, Susan MS. Image fusion of computed tomographic and magnetic resonance images for the development of a three-dimensional musculoskeletal model of the equine forelimb. *Vet Radiol Ultrasound*. 2006;47:553–62.